Performance Analysis of NOMA Assisted Underwater Visible Light Communication System

Monika Jain, Nikhil Sharma, *Member, IEEE*, Akash Gupta, *Member, IEEE*, Divyang Rawal, *Member, IEEE*, and Parul Garg, *Senior Member, IEEE*

***Abstract*—In this letter, we present the analytical investigation of the non-orthogonal multiple access (NOMA) assisted underwater visible light communication (UWVLC) system. The proposed system can cater to the needs such as low latency, high reliability and high data rate underwater multicasting to the sensor nodes. The UWVLC link is characterized by Exponential-Generalized Gamma (EGG) distribution. In particular, we derive the exact closed-form expressions of average bit error rate (BER) and ergodic capacity for underwater NOMA users. Further to understand the impact of the underwater scenario over the system performance, the analysis is carried out for parameters such as air bubble levels, gradient temperature and salinity level of the water. The obtained results validate the feasibility of the proposed system model.**

***Index Terms*—Non-orthogonal multiple access (NOMA), underwater visible light communication (UWVLC), bit error rate (BER), ergodic capacity.**

I. Introduction

IN THE recent past there has been an increase in underwater exploration, deployment of underwater wireless sensor networks and unmanned underwater vehicles, this has lead to an increase in the research interest towards the underwater communication [1]. The traditional underwater communication mostly banks on acoustic communication that suffers from low latency and low data rates [1]. Underwater visible light communication (UWVLC) using green and blue lasers has attracted the interest of researchers as a probable communication link serving the underwater communication bodies [2]. The performance of multi-user multiple-input multiple-output (MIMO)-orthogonal frequency division multiplexing (OFDM) has been analyzed in [3] for the underwater visible light communication system for the turbid water over the frequency selective channel. The authors in [4], considers the downlink of an underwater sensor network that builds upon the orthogonal frequency division multiple access (OFDMA)-based visible light communication system.

There has been an exponential increase in the number of underwater communication devices hence multiple access techniques have to be amalgamated in the communication model [5]. Non-orthogonal multiple access (NOMA) has evolved as a spectrally efficient, multiple access scheme that can cater to a large number of devices [6]. NOMA has been extensively studied in terrestrial radio frequency (RF) communication but limited studies have been done in underwater applications. The authors in [7], integrate the full duplex (FD) and NOMA with a relay based underwater acoustic network to improve the sum rate and reliability. A power allocation scheme for NOMA has been investigated in [8] for underwater acoustic communications. The analytical expressions for coverage probability and cell capacity is presented in [9] for weak underwater turbulence for the NOMA systems. The proposed work in this letter builts upon the idea of NOMA aided UWVLC by deriving the closed- form expressions of bit error rate (BER) and ergodic capacity at the near and far end users for different parameters like gradient temperature, bubble level (BL) and salinity of the water.

Motivated by the fact that none of the aforementioned work has depicted a NOMA assisted downlink UWVLC system, we propose and analyze this system to find its suitability as an efficient communication link between the on-surface and underwater communication bodies. To statistically analyze the proposed system model, we consider Exponential Generalized Gamma (EGG) fading model for the UWVLC system. We derive expressions for average BER and ergodic capacity in terms of a generalized Fox-H function. Further, we analyze our system for different underwater system parameters that statistically describe induced irradiance fluctuations for both weak as well as strong turbulence conditions taking into account both air BL and gradient temperature for fresh and salty water.

II. System and Channel Model

The system model of NOMA UWVLC consists of the underwater NOMA users, i.e., near-user UV_1 and far user (UV_2) at different height or distance from the on-surface floating vehicle (FV). The information symbols s_1 and s_2 are summed up after multiplying with their respective power allocation coefficients and then FV transmitted this superposition coded (SC) signal to both the underwater NOMA users through their respective links, i.e., FV $-$ UV_1 and

Manuscript received March 27, 2020; revised April 9, 2020; accepted April 14, 2020. Date of publication April 21, 2020; date of current version August 7, 2020. This work was supported by the Science and Engineering Research Board, Government of India under Project CRG/2018/002651. The associate editor coordinating the review of this article and approving it for publication was A. Liu. *(Corresponding author: Nikhil Sharma.)*

Monika Jain, Nikhil Sharma, Akash Gupta, and Divyang Rawal are with the Electronics and Communication Engineering Department, LNMIIT, Jaipur 302031, India (e-mail: monika.jain.y18pg@lnmiit.ac.in; nikhil.sharma@lnmiit.ac.in; akash.gupta@lnmiit.ac.in; divyang.rawal@lnmiit.ac.in).

Parul Garg is with the Division of Electronics and Communication Engineering, Netaji Subhas University of Technology, New Delhi 110078, India (e-mail: parul_saini@yahoo.co.in).

Digital Object Identifier 10.1109/LWC.2020.2988887

FV $-$ UV_2 which is assumed to be EGG distributed. The signal received by both the users over EGG channel is $y_{UV_i} = \eta I_i \hat{r}_{sc} + n_i, i = 1, 2$, where, η represents the responsivity, i.e., optical to electrical conversion coefficient, I_i indicates the real valued irradiance fluctuations for the corresponding link, n_i is the additive white Gaussian noise (AWGN) $\sim \mathcal{N}(0, \frac{N_o}{2})$ and $\hat{r}_{sc}$ is the transmitted superposition coded signal which is given as $\hat{r}_{sc} = \sqrt{\varphi_1} s_1 + \sqrt{\varphi_2} s_2$, where, φ_1 and φ_2 indicates the ratio of power allocated to UV_1 and UV_2, i.e., $\varphi_1 = \delta P_t$ and $\varphi_2 = (1-\delta) P_t$, wherein δ denotes the power allocation coefficient. P_t is the power transmitted by the source, s_1 and s_2 are on-off keying (OOK) modulated symbols for users UV_1 and UV_2, respectively. Without loss of generality, we consider that the channel gain for the near underwater vehicle/sensor node (UV_1) will be greater as compared to the far underwater vehicle/sensor node (UV_2), i.e., $|I_2|^2 < |I_1|^2$ where, I_2 and I_1 are the channel coefficients of (UV_2) and (UV_1), respectively. The user UV_2 which is the far NOMA user, decode its own symbol s_2 by employing maximum likelihood (ML) detection treating near user symbol s_1 as interference. On the other hand, user UV_1 which is the near NOMA user, decode its symbol s_1 by using successive interference cancellation (SIC) mechanism wherein, sequential decoding is performed by subtracting the regenerated symbol s_2 from the signal y_{UV_1}.

The UWVLC channel is statistically modeled by EGG distribution [2], the probability density function (PDF) is given as

$$f_\rho(\rho) = \frac{\omega_o}{r\rho} G_{0,1}^{1,0}\left[\frac{1}{\lambda_o}\left(\frac{\rho}{\mu_r}\right)^{\frac{1}{r}}\middle|\begin{matrix}-\\1\end{matrix}\right] + \frac{c_o(1-\omega)}{r\rho\Gamma(a_o)} G_{0,1}^{1,0}\left[\frac{1}{b_o^{c_o}}\left(\frac{\rho}{\mu_r}\right)^{\frac{c_o}{r}}\middle|\begin{matrix}-\\a_o\end{matrix}\right], \tag{1}$$

where, $\rho = \frac{(\eta I)^r}{N_o}$, N_o is the noise power, r depicts the detection technique involved, i.e., r=1 represents the heterodyne detection (HD) and r=2 represents intensity modulation/direct detection (IM/DD), ω_o is the mixture coefficient of Exponential and Generalized Gamma (GG) distributions, λ_o is the scale parameter of Exponential distribution, while a_o, b_o and c_o are parameters of GG distribution for different underwater scenarios, $\Gamma(.)$ represents the Gamma function and μ_r is a function of average electrical signal-to-noise-ratio (SNR) as given in [2].

III. Performance Analysis

In this section, we derive the exact closed-form expressions of the average BER and ergodic capacity for the underwater NOMA near user (UV_1) and far user (UV_2).

A. Average BER Analysis

The signal space constellation received by NOMA far user UV_2 and near user UV_1 is shown in Fig. 1(a) and Fig. 1(b), respectively. The Fig. 1 depicts decision boundary and hence erroneous detections. Green line depicts correct decision while red line depicts erroneous one. The symbol (s_1, s_2) consists of individual bits of near and far user, respectively. Table I elaborates Fig. 1 with decision boundary for every cases that can occur. The decision boundary for far user UV_2 for computing the BER is Q_1 as shown in Fig. 1(a). The instantaneous

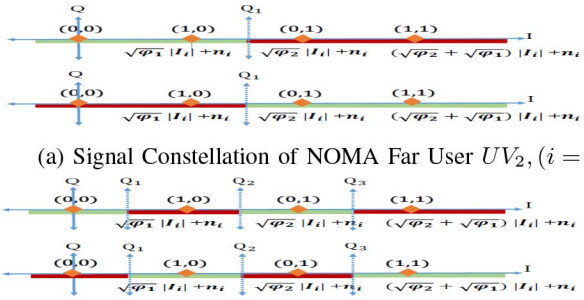

(a) Signal Constellation of NOMA Far User $UV_2, (i = 2)$.

(b) Signal Constellation of NOMA Near User $UV_1, (i = 1)$.

Fig. 1. Signal Space representation of NOMA assisted UWVLC system for OOK modulation scheme.

BER of far user is the sum of individual BER of each constellation point multiplied by their respective prior probabilities which are equiprobable. The bit $s_2 = 0$ of symbol (0, 0) and (1, 0) is erroneously detected as $s_2 = 1$ to the right side of Q_1. Similarly, bit $s_2 = 1$ of symbol (0, 1) and (1, 1) is mistakenly identified as $s_2 = 0$ to the left side of Q_1. The PDF of constellation point (0, 0) can be expressed as $f_{0,0} = \frac{1}{\sqrt{2\pi\sigma^2}} \exp \frac{-(x-0)^2}{2\sigma^2}$. The error probability of point (0, 0) is written as $P_{UV_{2|(0,0)}} = \int_{\sqrt{\frac{\rho_1}{2}}}^{\infty} \exp \frac{-(x-0)^2}{(\sqrt{N_o})^2} dx = \mathcal{Q}(\sqrt{\rho_1})$, where, $\mathcal{Q}(.)$ denotes $\mathcal{Q}$-function, $\rho_1 = \frac{(\sqrt{\varphi}_2 + \sqrt{\varphi}_1)^2 |I_2|^2}{2N_o}$. Applying similar mathematical procedure, we can obtain BER for individual constellation points. The total instantaneous BER of far user UV_2 can be written as

$$P_{UV_2} = \frac{1}{4}[2\mathcal{Q}(\sqrt{\rho_1}) + 2\mathcal{Q}(\sqrt{\rho_2}) - \mathcal{Q}(\sqrt{\rho_3}) - \mathcal{Q}(\sqrt{\rho_4})], \tag{2}$$

where, $\rho_2 = \frac{(\sqrt{\varphi}_2 - \sqrt{\varphi}_1)^2 |I_2|^2}{2N_o}, \rho_3 = \frac{2\varphi_2 |I_2|^2}{N_o}$ and $\rho_4 = \frac{2(\sqrt{\varphi}_2 + \sqrt{\varphi}_1)^2 |I_2|^2}{N_o}$. The decision boundary for near user UV_1 for computing the BER are Q_1, Q_2 and Q_3 as shown in Fig. 1(b). It is worth mentioning that the error region on the right region of axis Q3 for point (0, 0) and the region [Q2, Q3] for point (1, 0) can be attributed to the NOMA error propagation (error incurred during detection of far user (UV_2) bits) resulting from the decoding error of near user (UV_1). The instantaneous BER of near user is obtained by the summation of individual error probabilities of each constellation symbol multiplied by its prior probability which is given as

$$\begin{aligned} P_{UV_1} = \frac{1}{4}[&\mathcal{Q}(\sqrt{\rho_5}) + 3\mathcal{Q}(\sqrt{\rho_6}) - \mathcal{Q}(\sqrt{\rho_7}) + 2\mathcal{Q}(\sqrt{\rho_8}) \\ &- 2\mathcal{Q}(\sqrt{\rho_9}) + \mathcal{Q}(\sqrt{\rho_{10}}) - \mathcal{Q}(\sqrt{\rho_{11}}) - \mathcal{Q}(\sqrt{\rho_{12}})], \end{aligned} \tag{3}$$

$$\begin{aligned} &\text{where, } \rho_5 = \frac{\left(-\sqrt{\varphi}_2 + \sqrt{\varphi}_1\right)^2 |I_1|^2}{2N_o}, \rho_6 = \frac{\varphi_1 |I_1|^2}{2N_o}, \\ &\rho_7 = \frac{2\varphi_1 |I_1|^2}{N_o}, \rho_8 = \frac{\left(\sqrt{\varphi}_2 - \sqrt{\varphi}_1\right)^2 |I_1|^2}{2N_o}, \\ &\rho_9 = \frac{\left(2\sqrt{\varphi}_2 - \sqrt{\varphi}_1\right)^2 |I_1|^2}{2N_o}, \rho_{10} = \frac{\left(2\sqrt{\varphi}_2 + \sqrt{\varphi}_1\right)^2 |I_1|^2}{2N_o}, \\ &\rho_{11} = \frac{2\left(\sqrt{\varphi}_2 - \sqrt{\varphi}_1\right)^2 |I_1|^2}{2N_o}, \rho_{12} = \frac{\left(\sqrt{\varphi}_2 + \sqrt{\varphi}_1\right)^2 |I_1|^2}{2N_o}. \end{aligned} \tag{4}$$

TABLE I
DECISION BOUNDARIES FOR UV_1 AND UV_2 FOR ALL CONSTELLATION POINTS

Transmitted Symbol (s_1, s_2)	**Erroneous detection & decision regions for** UV_2		**Erroneous detection & decision regions for** UV_1	
(0,0)	(0,1)	Right of Q_1	(1,0)	Q_1 to Q_2
	(1,1)	Right of Q_1	(1,1)	Right of Q_3
(1,0)	(0,1)	Right of Q_1	(0,0)	Left of Q_1
	(1,1)	Right of Q_1	(0,1)	Q_2 to Q_3
(0,1)	(0,0)	Left of Q_1	(1,0)	Q_1 to Q_2
	(1,0)	Left of Q_1	(1,1)	Right of Q_3
(1,1)	(0,0)	Left of Q_1	(0,0)	Left of Q_1
	(1,0)	Left of Q_1	(0,1)	Q_2 to Q_3

Utilizing (1) and the identities $\mathcal{Q}(x) = \frac{1}{2}erfc(\frac{x}{\sqrt{2}})$, $erfc(\sqrt{x}) = \frac{1}{\sqrt{\pi}}G_{1,2}^{2,0}\left[x|\begin{matrix}1\\0,\frac{1}{2}\end{matrix}\right]$; we can derive the average BER as $\bar{P}_{UV_i} = \int_0^\infty P_{UV_i} f_\rho(\rho)d\rho$. The integral is further solved using the identities [10, eq. (8.4.51/9)], [11, eqs. (2.8.4) and (2.9.1)]. The closed-form expression of average BER for near and far user is shown in (5), at the bottom of the page.

B. Ergodic Capacity Analysis

The sum rate of NOMA UWLC system is given as

$$C_{sum} = \sum_{i=1}^{2} C_{UV_i}, i = 1, 2 \tag{6}$$

where, $C_{UV_i} = E[\ln(1 + \varsigma\rho_{UV_i})]$, $i\epsilon\{1, 2\}$ denotes the ergodic capacity at the near and far NOMA assisted users respectively as defined in [2] and $\varsigma = \frac{e}{2\pi}$. The closed-form expression of the ergodic capacity is obtained by solving C_{UV_i} with the help of (1) and the identities [10, eqs. (8.4.6/5) and (8.4.51/9)] and [11, eqs. (2.8.4) and (2.1.4)]. The ergodic capacity of the near and far users for a NOMA assisted UWVLC system is shown in (7), at the bottom of the page.

IV. NUMERICAL RESULTS AND DISCUSSIONS

In this section, the performance of the considered UWVLC system in terms of average BER and ergodic capacity is evaluated for IM/DD (r = 2). The UWVLC link experiences EGG turbulence due to induced air bubble levels and gradient temperature for different values of ω_o, λ_o, a_o, b_o and c_o for both fresh and saline water sources as listed in [2, Tables I and II]. The average channel variance for user UV_1 and UV_2 are considered as $E[|I_1|^2] = 0$dB and $E[|I_2|^2] = -3$dB, respectively.

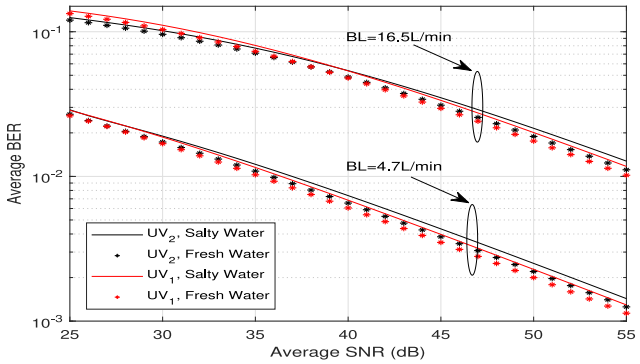

Fig. 2. Average BER versus SNR for different salinity and bubble levels, $\delta = 0.3$.

In Fig. 2, we explore the dependence of average BER of system on salinity and BL of the water. Interestingly, it is observed that the effect of BL is more dominant over the system performance as compared to the effect of salinity of the water. This is because as the air BL increases, the value of scintillation index also rises due to severe fluctuations in the intensity of the received signal. Further, as the BL increases the cut-off SNR for which the system performance is dominated by the channel condition instead of the transmit power also increases. To support this statement, it is clearly observed that the above mentioned cut-off SNR in case of BL = 4.7 L/min is 25 dB, which increases to 40 dB for BL =16.5 L/min.

The BER performance of far user UV_2 w.r.t SNR for different gradient temperature and power allocation coefficient is presented in Fig. 3. The power allocated to the far user is $(1 - \delta)P_t$, hence with the decrease in power allocation coefficient the transmitted power increases thereby improving the error performance. The same been validated in Fig. 3, for example at SNR = 50 dB the average BER = 0.009258 for $\delta = 0.4$ and gradient temperature equals to 0.15 $^\circ C/cm$ and it increases to 0.004237 for $\delta = 0.25$ at the same gradient temperature. The similar trend can be verified for the variation in gradient temperature.

$$\bar{P}_{UV_1} = \frac{1}{4}[\mathbb{X}(\bar{\rho}_5) + 3\mathbb{X}(\bar{\rho}_6) - \mathbb{X}(\bar{\rho}_7) + 2\mathbb{X}(\bar{\rho}_8) - 2\mathbb{X}(\bar{\rho}_9) + \mathbb{X}(\bar{\rho}_{10}) - \mathbb{X}(\bar{\rho}_{11}) - \mathbb{X}(\bar{\rho}_{12})], \bar{P}_{UV_2} = \frac{1}{4}[2\mathbb{X}(\bar{\rho}_1) + 2\mathbb{X}(\bar{\rho}_2) - \mathbb{X}(\bar{\rho}_3) - \mathbb{X}(\bar{\rho}_4)]$$

$$where,\ \mathbb{X}(\bar{\rho}_j) = \frac{\omega_o}{2\sqrt{\pi}}H_{2,2}^{1,2}\left[\frac{2}{\lambda_o^r\mu_r}\middle|\begin{matrix}(1,1),(\frac{1}{2},1)\\(1,r),(0,1)\end{matrix}\right] + \frac{(1-\omega_o)}{2\sqrt{\pi}\Gamma(a_o)}H_{2,2}^{1,2}\left[\frac{2}{b_o^r\mu_r}\middle|\begin{matrix}(1,1),(\frac{1}{2},1)\\(a_o,\frac{r}{c_o}),(0,1)\end{matrix}\right], \mu_r = \frac{\bar{\rho}_j}{2\omega_o\lambda_o^2 + b_o^2(1-\omega_o)\Gamma(a_o+2/c_o)/\Gamma(a_o)},$$

$$\bar{\rho}_j = E\{\rho_j\},\ j\epsilon\{1,2,3,4\} \text{ for NOMA far user, } j\epsilon\{5,6,7,8,9,10,11,12\} \text{ for NOMA near user and E is the expectation operator} \tag{5}$$

$$C_{UV_i} = \omega_o H_{2,3}^{3,1}\left[\frac{1}{\lambda_o^r\varsigma\mu_r}\middle|\begin{matrix}(0,1),(1,1)\\(1,r),(0,1),(0,1)\end{matrix}\right] + \frac{(1-\omega_o)}{\Gamma(a_o)}H_{2,3}^{3,1}\left[\frac{1}{b_o^r\varsigma\mu_r}\middle|\begin{matrix}(0,1),(1,1)\\(a_o,\frac{r}{c_o}),(0,1),(0,1)\end{matrix}\right]$$

$$\text{where } \mu_r = \mu_2 = \frac{\bar{\rho}_{UV_i}}{2\omega_o\lambda_o^2 + b_o^2(1-\omega_o)\Gamma(a_o+2/c_o)/\Gamma(a_o)}, i = 1, 2 \text{ and } \bar{\rho}_{UV_1} = \frac{\delta P_t E\left[|I_1|^2\right]}{N_o}, \bar{\rho}_{UV_2} = \frac{(1-\delta)P_t E\left[|I_2|^2\right]}{\delta P_t E\left[|I_2|^2\right] + N_o} \tag{7}$$

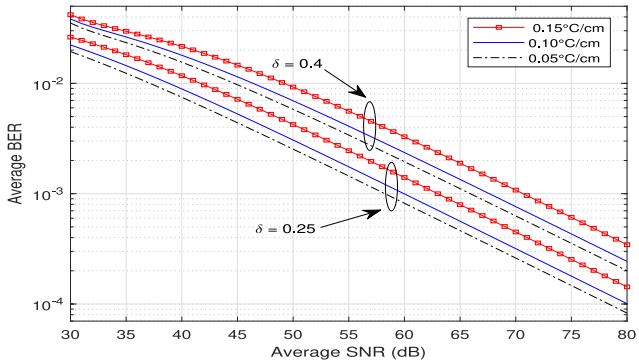

Fig. 3. Average BER versus SNR for far user UV_2 at BL = 2.4 L/min and gradient temperature, $\delta = 0.4$.

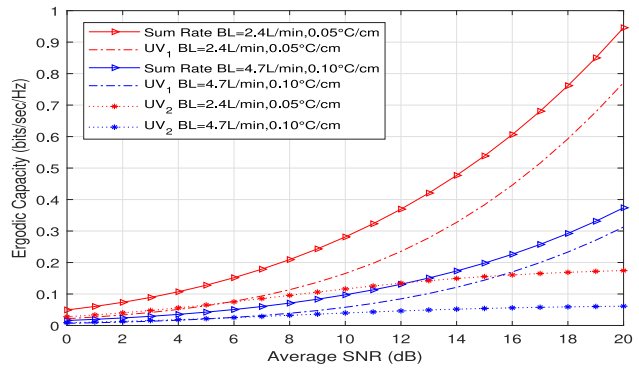

Fig. 4. Ergodic Capacity versus SNR at BL = 2.4 L/min, 4.7 L/min and gradient temperature, $\delta = 0.25$.

The Fig. 4 demonstrates the result of ergodic capacity for different gradient temperature, i.e., 0.05 $^{\circ}C/cm$, 0.10 $^{\circ}C/cm$ and different air bubble levels, i.e., 2.4 L/min and 4.7 L/min for both near and far NOMA users. Further, their corresponding sum rates is also presented. Fig. 4 clearly demonstrates the impact of the air BL and gradient temperature on the performance of system. With increase in the BL and gradient temperature it is clearly observed that there is detrimental effect on the ergodic capacity of the system. The severity of this effect is more for near user as compared to that of the far user For instance, a gain of 0.458 bits/sec/Hz is observed at 20 dB as BL decreases from 4.7 L/min to 2.4 L/min for near user (UV_1), similarly a gain of 0.113 bits/sec/Hz is observed in case of far user (UV_2).

Fig. 5, demonstrates a comparative analysis of the ergodic capacity for fresh and salty water scenarios at a bubble level of 4.7 L/min. It can been seen from Fig. 5, that as the salinity level gets increased, severe fluctuations occur in the intensity of received signal due to which scintillation index tends to increase, therefore average BER increases leading to a degradation in the system performance. Thus, higher the salinity lower is the performance of underwater system. A gain of 0.639 bits/sec/Hz is observed at 20 dB with decrease in the salinity of water from salty to fresh. Another interesting observation from Fig. 4 and Fig. 5 is that the ergodic capacity of far user saturates beyond a particular SNR which is due to the fact that at lower SNRs the interference due to near user is less because of the dominant nature of the transmitted

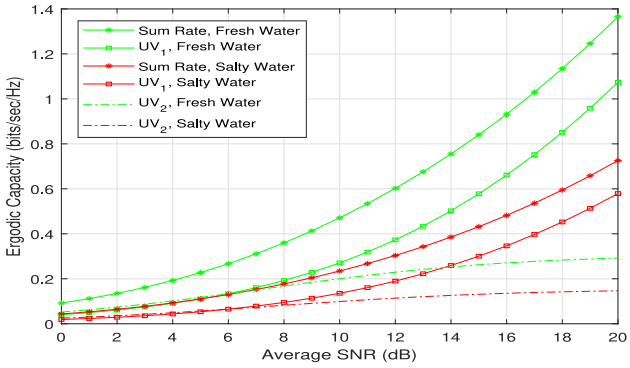

Fig. 5. Ergodic Capacity versus SNR at BL = 4.7 L/min for fresh and salty water sources, $\delta = 0.25$.

power and the situation reverses at higher SNR values where the interference due to near user is more and suppresses the ergodic capacity of the far user.

V. Conclusion and Future Works

In this letter, we derive the novel closed-form expressions of average BER and ergodic capacity in terms of Fox-H function for both NOMA near and far users. The performance of the system is analyzed for different underwater scenarios such as BL, salinity of water, and gradient temperature. Thus, it is concluded that the results can assist system designers for selecting parameters to suit their water ecosystem. As a part of future work the analysis can be extended to 'N' number of NOMA users in UWVLC scenario.

References

[1] Z. Zeng, S. Fu, H. Zhang, Y. Dong, and J. Cheng, "A survey of underwater optical wireless communications," *IEEE Commun. Surveys Tuts.*, vol. 19, no. 1, pp. 204–238, 1st Quart., 2017.

[2] E. Zedini, H. M. Oubei, A. Kammoun, M. Hamdi, B. S. Ooi, and M. Alouini, "Unified statistical channel model for turbulence-induced fading in underwater wireless optical communication systems," *IEEE Trans. Commun.*, vol. 67, no. 4, pp. 2893–2907, Apr. 2019.

[3] A. Amantayeva, M. Yerzhanova, and R. C. Kizilirmak, "Multiuser MIMO for underwater visible light communication," in *Proc. IEEE Int. Conf. Comput. Netw. Commun. (CoCoNet)*, Aug. 2018, pp. 164–168.

[4] M. Elamassie, M. Karbalayghareh, F. Miramirkhani, M. Uysal, M. Abdallah, and K. Qaraqe, "Resource allocation for downlink OFDMA in underwater visible light communications," in *Proc. IEEE Int. Black Sea Conf. Commun. Netw. (BlackSeaCom)*, Jun. 2019, pp. 1–6.

[5] M. J. Bocus, D. Agrafiotis, and A. Doufexi, "Non-orthogonal multiple access (NOMA) for underwater acoustic communication," in *Proc. IEEE 88th Veh. Technol. Conf. (VTC-Fall)*, Chicago, IL, USA, 2018, pp. 1–5.

[6] M. Jain, S. Soni, N. Sharma, and D. Rawal, "Performance analysis at far and near user in NOMA based system in presence of SIC error," *AEU Int. J. Electron. Commun.*, vol. 114, Feb. 2020, Art. no. 152993.

[7] E. A. Makled, A. Yadav, O. A. Dobre, and R. D. Haynes, "Hierarchical full-duplex underwater acoustic network: A NOMA approach," in *Proc. OCEANS MTS/IEEE Charleston*, Oct. 2018, pp. 1–6.

[8] J. Cheon and H.-S. Cho, "Power allocation scheme for non-orthogonalmultiple access in underwater acoustic communications," *Sensors*, vol. 17, no. 11, pp. 2465–2478, Oct. 2017.

[9] C. Geldard, J. Thompson, and W. O. Popoola, "A study of non-orthogonal multiple access in underwater visible light communication systems," in *Proc. IEEE 87th Veh. Technol. Conf. (VTC)*, Porto, Portugal, 2018, pp. 1–6.

[10] A. Prudnikov, Y. Brychkov, and O. Marichev, *Integrals and Series, Volume 3: More Special Functions*. Boca Raton, FL, USA: CRC Press, 1999.

[11] A. Kilbas and M. Saigo, *H-Transforms: Theory and Applications*. (Analytical Method and Special Function), 1st ed. Boca Raton, FL, USA: CRC Press, 2004.